Multiple energy x–ray holography: the polarization effect

V. Bortolani

INFM and Dipartimento di Fisica, Università di Modena, via Campi 213/A, I-41100 Modena, Italy.

V. Celli

Physics Department, University of Virginia, Charlottesville, Virginia 22904–4714.

A. M. Marvin

Dipartimento di Fisica Teorica, Università di Trieste, Miramare–Grignano, I-34014 Trieste, Italy.

Abstract

We present the theory for Multiple Energy X–ray Holography (MEXH), using a multipole expansion for the scattered field. We find that light polarization plays a crucial role in the reconstruction of the image, and we suggest how to use it in order to eliminate aberration effects. The method we propose is alternative to the SWIFT method (*scattered-wave–included Fourier transform*), but has the advantage that no theoretical calculations are required to redefine the hologram.

PACS 42.40.-i

I. INTRODUCTION.

The idea of holography dates back to Gabor's original works[1] and is essentially based on the interference of optical paths in crystal diffraction. The problem has been summarized very clearly by Szöke[2]. Consider as a simple example, an emitter A at the origin and a single neighbouring atom N_1 at a position $\mathbf{r}_1$. In the process known as *x–ray fluorescence holography* (XFH)[3,4], the atom A is excited and the emitted radiation either goes directly to the detector (photofilm) at a far distance R (the so called *reference wave*), or is firstly scattered by N (*object wave*). The photofilm registers in this way the interference of the two optical paths (hologram), and gets in Fourier transform the desired information on the scatterer position $\mathbf{r}_1$. Equivalently, as proposed originally by Gabor[1], the last step can be accomplished by illuminating the photographic film with an incoming spherical wave[2,5] (the *decoding wave*), but numerical solutions that use a digital detector and suppress the decoding wave are nowadays preferable.

A step forward in this direction has been given recently by the group of Fadley and Materlik[6], in using the emitter A as a detector. In this experiment (MEXH), the reference wave is furnished by a synchrotron radiation (SR) source, while the fluorescing atom A senses an electric field which is the sum of the direct wave and the scattered front (see Fig. 1) due to its neighbouring atoms (*object wave*).

Formally, MEXH can be visualized as a time reversal situation of XFH, in the sense that the detector is substituted by the source, which obviously does *not* modify the hologram. In spite of this, it presents many hidden advantages.

First of all, the hologram $\chi(\mathbf{k})$ is defined at different energies. In MEXH and in contrast to XFH, the photon energy is always above the fluorescence threshold of the emitter, thus allowing a better resolution of the image as $\sim k^{-1}$. Secondly, the SR photon energy in MEXH can be freely varying, and this allows one to suppress unpleasant *twin–image* effects, once the integration is not limited to a sphere, but is done over a a 3–D volume in $\mathbf{k}$ space[7]. A comparison between the two methods has been given recently by Len *et al.*[8] and we refer

to them for further details.

In this report we develop the full vector theory for MEXH. The general theory is presented in section II. In Sec. III we make a multipole expansion of the previous formulae, and discuss their limit of applicability. Here is where aberration comes out, and we show in Sec. IV how to avoid it, playing with the polarization of the reference beam. Finally in Sec. V we confirm our previous findings presenting some numerical results on a real crystal structure. Particular attention is devoted to the disturbance induced by the scatterers at the large distance from the emitter.

II. THE BASIC EQUATIONS.

Let us fix our attention on the neighbouring atoms first. The external SR monochromatic field is represented by the *normalized* vector potential

$$\mathbf{A}(\mathbf{r},\, t) = \boldsymbol{\epsilon}\, e^{i\mathbf{k}\cdot\mathbf{r}} e^{-i\omega t} + \quad c.c. \tag{2.1}$$

where $k = \omega/c$ and $\boldsymbol{\epsilon}$ is the polarization. This acts on each atom surrounding A as a disturbance $H_I \sim -e\mathbf{A}\cdot\mathbf{p}$, causing a transition on the electronic states. The density and current involved in this process are

$$\rho \sim -e\, \psi_n^* \psi_m + (m \leftrightarrow n) \tag{2.2a}$$

$$\mathbf{j} \sim \frac{-e}{m} \times \left[\frac{-i\hbar}{2} \left(\psi_n^* \nabla\psi_m - \psi_m \nabla\psi_n^*\right) + (m \leftrightarrow n) + \frac{e}{c}|\psi_n|^2 \right], \tag{2.2b}$$

where ψ_n is the initial core electron level, ψ_m is the final state, and the last term in (2.2b) is the diamagnetic contribution. Each transition is then weighted by appropriate coefficients, which can be found by applying standard perturbation theory.[9] Matching the density and the current density operators between states, the result is of the same form as in Eq. (2.1), i.e.

$$\rho(\mathbf{r},\, t) = \rho(\mathbf{r};\, \omega) e^{-i\omega t} + \quad c.c. \tag{2.3a}$$

and

$$\mathbf{j}(\mathbf{r},\, t) = \mathbf{j}(\mathbf{r};\, \omega)e^{-i\omega t} + \quad c.c. \tag{2.3b}$$

To find the two quantities on the r.h.s., we must pay attention that: 1) the atoms are centered at $\mathbf{r}_s$ and *not* at the origin; 2) the wavefunctions ψ depend on the relative position with respect to the nucleus

$$\mathbf{x} = \mathbf{r} - \mathbf{r}_s \tag{2.4}$$

and are otherwise independent of s. This means that the induced density (or current) for each atom, factorizes as a prefactor $\exp(i\mathbf{k}\cdot\mathbf{r}_s)$ times a term which is function of $\mathbf{x}$ in Eq. (2.4) and is *formally* independent of the atomic position. The total induced density (or current) is the sum over atoms. With this in mind the result is

$$\rho(\mathbf{r};\, \omega) = \sum_s e^{i\mathbf{k}\cdot\mathbf{r}_s}\, \rho(\mathbf{x}) \quad ; \quad \mathbf{j}(\mathbf{r};\, \omega) = \sum_s e^{i\mathbf{k}\cdot\mathbf{r}_s}\, \mathbf{j}(\mathbf{x}) \tag{2.5}$$

where

$$\begin{aligned}\rho(\mathbf{x}) = -\frac{e^2}{mc}\sum_{\beta=1}^{3}\sum_m \Bigg[&-\frac{\psi_n^{(0)^*}(\mathbf{x})\psi_m^{(0)}(\mathbf{x})\langle m|e^{i\mathbf{k}\cdot\mathbf{x}'}p_\beta|n\rangle}{\hbar(\omega_{mn} - \omega - i\delta)} \\ &-\frac{\langle n|e^{i\mathbf{k}\cdot\mathbf{x}'}p_\beta|m\rangle\psi_m^{(0)^*}(\mathbf{x})\psi_n^{(0)}(\mathbf{x})}{\hbar(\omega_{mn} + \omega - i\delta)}\Bigg]\, \epsilon_\beta,\end{aligned} \tag{2.6}$$

and

$$\begin{aligned}j_\alpha(\mathbf{x}) = -\frac{e^2}{mc}\sum_{\beta=1}^{3}\Bigg\{ &\delta_{\alpha\beta}e^{i\mathbf{k}\cdot\mathbf{x}}|\psi_n^{(0)}(\mathbf{x})|^2 - \frac{1}{m}\sum_m \Bigg[\\ &\frac{\psi_n^{(0)^*}(\mathbf{x})\ \overleftrightarrow{p_\alpha}\ \psi_m^{(0)}(\mathbf{x})\langle m|e^{i\mathbf{k}\cdot\mathbf{x}'}p_\beta|n\rangle}{\hbar(\omega_{mn} - \omega - i\delta)} \\ &+\frac{\langle n|e^{i\mathbf{k}\cdot\mathbf{x}'}p_\beta|m\rangle\psi_m^{(0)^*}(\mathbf{x})\ \overleftrightarrow{p_\alpha}\ \psi_n^{(0)}(\mathbf{x})}{\hbar(\omega_{mn} + \omega - i\delta)}\Bigg]\Bigg\}\epsilon_\beta.\end{aligned} \tag{2.7}$$

In Eq. (2.7) the dyadic over the momentum operator, $\mathbf{p} = -i\hbar\nabla$, means that it operates symmetrically both on the right and on the left, according to the square bracket in Eq. (2.2b). In the first row in Eq. (2.7) one recognizes the diamagnetic contribution which does not depend on the virtual states m, while in the denominators we have defined

$$\omega_{mn} = \left(E_m^{(0)} - E_n^{(0)}\right)/\hbar,$$

and $E_{m,n}^{(0)}$ are energies of the excited and core electron level. It can be verified from (2.6) and (2.7) that Eq. (2.3a) and Eq. (2.3b) satisfy the charge conservation $\nabla \cdot \mathbf{j} + \dot{\rho} = 0$. Once the charges and currents are given, the electric field at the emitter is calculated from the Maxwell equations. Outside the sources, this can be found from the vector potential only as

$$\mathbf{E} = \frac{i}{k}\nabla \times \mathbf{B} \quad ; \quad \mathbf{B} = \nabla \times \mathbf{A} \tag{2.8}$$

where

$$\mathbf{A}(\mathbf{r};\,\omega) = \frac{1}{c}\int \frac{e^{ik|\mathbf{r}-\mathbf{r}'|}}{|\mathbf{r}-\mathbf{r}'|}\mathbf{j}(\mathbf{r}';\,\omega)\,d^3\mathbf{r}'.$$

Changing the integration variable as in Eq. (2.4), then using the definition in (2.5), one gets

$$\mathbf{E}_{\rm obj}(\mathbf{r};\,\omega) = \frac{i}{\omega}\sum_s e^{i\mathbf{k}\cdot\mathbf{r}_s}\Bigg\{\nabla\times \int\left[\left(\nabla\frac{e^{ik|\mathbf{r}-\mathbf{r}_s-\mathbf{x}'|}}{|\mathbf{r}-\mathbf{r}_s-\mathbf{x}'|}\right)\times\mathbf{j}(\mathbf{x}')\right]\,d^3\mathbf{x}'\Bigg\}. \tag{2.9}$$

The last equation is the object wave due to the scatterers. A similar result has been obtained recently by Fonda[10] by computing the field through the vector and scalar potentials, but erroneously the latter was neglected from the start. Fonda's result, in the present notation, is $\mathbf{E}_{\rm obj} = ik\mathbf{A}$, which is equivalent to dropping one term of the double vector product in Eq. (2.9). Further on, we show in Sec. IV how this correction becomes crucial for the polarization dependence of the reconstructed image, which is the main point of this paper.

Adding from (2.1) the direct contribution of the reference wave, i.e.,

$$\mathbf{E}_{\rm ref}(\mathbf{r};\,\omega) = ik\boldsymbol{\epsilon}\,e^{i\mathbf{k}\cdot\mathbf{r}}, \tag{2.10}$$

we get the total field

$$\mathbf{E}_{\rm Tot} = \mathbf{E}_{\rm ref} + \mathbf{E}_{\rm obj} \tag{2.11}$$

that acts as a perturbation on the fluorescing atom A.

III. THE MULTIPOLE EXPANSION.

The states of A involved in the transition are again core electron levels. This means that one needs Eq. (2.11) for $\mathbf{r} = \mathbf{x}$ and $|\mathbf{x}| \lesssim d$, with d of the order of the Bohr radius. In the same way, the integral in Eq. (2.9) is confined to $|\mathbf{x}'| \lesssim d$, i.e., in the volume where the current in (2.2b) is appreciably different from zero. Since r_s is of the order of the lattice parameter, it follows that

$$r_s \gg x,\, x'.$$

This allows us to use for the propagator in Eq. (2.9) the so called plane wave approximation (PWA)[10]

$$\frac{e^{ik|\mathbf{r}-\mathbf{r}_s-\mathbf{x}'|}}{|\mathbf{r}-\mathbf{r}_s-\mathbf{x}'|} \approx \frac{e^{ik|\mathbf{r}-\mathbf{r}_s|}}{|\mathbf{r}-\mathbf{r}_s|}\, e^{-i\mathbf{k}_s\cdot\mathbf{x}'} \tag{3.1}$$

with $\mathbf{k}_s = -k\hat{\mathbf{r}}_s$ the scattered momentum. One gets

$$\begin{aligned}\mathbf{E}_{\rm obj}(\mathbf{x};\,\omega) = \sum_s k^2 e^{i\mathbf{k}_s\cdot\mathbf{x}} \Bigg\{ &[\mathbf{M}_s - (\mathbf{M}_s\cdot\hat{\mathbf{r}}_s)\hat{\mathbf{r}}_s] \\ &+ \frac{1}{ikr_s}[3(\mathbf{M}_s\cdot\hat{\mathbf{r}}_s)\hat{\mathbf{r}}_s - \mathbf{M}_s]\left(1 - \frac{1}{ikr_s}\right)\Bigg\}\frac{e^{ikr_s}}{r_s}\, e^{i\mathbf{k}\cdot\mathbf{r}_s}\end{aligned} \tag{3.2}$$

with

$$\mathbf{M}_s = \frac{i}{\omega}\int e^{-i\mathbf{k}_s\cdot\mathbf{x}'}\mathbf{j}(\mathbf{x}')\, d^3\mathbf{x}'. \tag{3.3}$$

Eq. (3.2) has been written for completeness. For $kd \ll 1$, $\exp(-i\mathbf{k}_s\cdot\mathbf{x}') \approx 1$ in Eq. (3.3) and $\mathbf{M}_s \approx \mathbf{p}$,[11] with

$$\mathbf{p} = \int \mathbf{x}'\rho(\mathbf{x}')\, d^3\mathbf{x}' \tag{3.4}$$

the electric dipole moment, and ρ the density in Eq. (26). In this case the object field in (3.2) is constant over the atom. In the two extreme limits $kr_s \gg 1$ and $kr_s \ll 1$ one discovers in it the familiar result (see Ref. [11]) of the radiative and the near static field in the dipole approximation.

For x–rays the limit $kr_s \gg 1$ is appropriate, but $k \sim d^{-1}$ is required for good resolution. This means that under the sum in (3.2) only the first term is contributes, while in Eq. (3.3) one is led to attempt an expansion as

$$e^{-i\mathbf{k}_s\cdot\mathbf{x}'} \approx 1 - i\mathbf{k}_s\cdot\mathbf{x}' + \cdots$$

The result is

$$\begin{aligned}\mathbf{E}_{\rm obj}(\mathbf{x};\,\omega) = \sum_s k^2 e^{i\mathbf{k}_s\cdot\mathbf{x}}\Big\{ &[-\hat{\mathbf{r}}_s\times(\hat{\mathbf{r}}_s\times\mathbf{p})] \\ &+ [\hat{\mathbf{r}}_s\times\mathbf{m}] - \frac{i}{3!}\,[-\hat{\mathbf{r}}_s\times(\hat{\mathbf{r}}_s\times\mathbf{Q}_s)]\Big\}\frac{e^{ikr_s}}{r_s}e^{i\mathbf{k}\cdot\mathbf{r}_s}\end{aligned} \tag{3.5}$$

where $\mathbf{m}$ is the magnetic dipole moment,

$$(\mathbf{Q}_s)_\alpha = \sum_{\beta=1}^{3} Q_{\alpha\beta}\,(\mathbf{k})_\beta\,, \tag{3.6a}$$

and $Q_{\alpha\beta}$ is the electric quadrupole moment tensor

$$Q_{\alpha\beta} = \int \left(3x'_\alpha x'_\beta - {r'}^2\delta_{\alpha\beta}\right)\,\rho(\mathbf{x}')\,d^3\mathbf{x}'. \tag{3.6b}$$

To make the expansion consistent, we shall suppose in the following that the last two terms in Eq. (3.5) are small. Equally well we shall suppose that the same happens for the fluorescing atom A, such that the limit $\mathbf{x} = 0$ in Eq. (35) is appropriate. The yield is simply $\sim |\mathbf{E}(\mathbf{x} = 0)|^2$ and function of the direction $\hat{\mathbf{k}}$ of the laser beam only. The hologram follows as

$$\chi(\mathbf{k}) = \left(|\mathbf{E}_{\rm Tot}|^2 - |\mathbf{E}_{\rm ref}|^2\right)/|\mathbf{E}_{\rm ref}|^2 \tag{3.7a}$$

$$\approx \frac{1}{k^2}\,(\mathbf{E}^*_{\rm ref}\cdot\mathbf{E}_{\rm obj} + \quad c.c.) \tag{3.7b}$$

and in the last line the *self–hologram* $\sim \mathbf{E}^2_{\rm obj}$ has been neglected. Using (2.10) and (3.4) the result for Eq. (3.7b) is

$$\chi(\mathbf{k}) = -ik\sum_s f_s\frac{e^{ikr_s}}{r_s}e^{i\mathbf{k}\cdot\mathbf{r}_s} + \quad c.c. \tag{3.8}$$

and where f_s the scattering amplitude

$$f_s = (\boldsymbol{\epsilon}^* \times \hat{\mathbf{r}}_s) \cdot (\mathbf{p} \times \hat{\mathbf{r}}_s) + \boldsymbol{\epsilon}^* \times \mathbf{r}_s \cdot \mathbf{m} - \frac{i}{3!} (\boldsymbol{\epsilon}^* \times \mathbf{r}_s) \cdot (\mathbf{Q}_s \times \hat{\mathbf{r}}_s) \,. \tag{3.9}$$

Equation above shows that f_s is complex and is polarization dependent. The quadrupole correction, causes a shift[8], while the dipole terms give rise to a distortion of the image (*aberration effects*). In practical cases (see Ref. [8] for details) the shift is $\sim 1/10$ of the resolution and thus negligible. On the contrary the distortion is effective and is polarization dependent.

IV. ANGULAR ANISOTROPIES.

For a constant f_s in Eq. (3.8), the Fourier transform

$$U(\mathbf{r};\, k) = \frac{1}{4\pi} \int \chi(\mathbf{k}) e^{-i\mathbf{k}\cdot\mathbf{r}} \, d\hat{\mathbf{k}}, \tag{4.1}$$

with $d\hat{\mathbf{k}}$ denoting the solid angle $d\Omega_{\mathbf{k}}$, solves completely the problem of the atomic position. In this case[2]

$$U(\mathbf{r};\, k) = -ik \sum_s f_s \frac{e^{ikr_s}}{r_s} \frac{\sin(k|\mathbf{r} - \mathbf{r}_s|)}{k|\mathbf{r} - \mathbf{r}_s|} + ik \sum_s f_s^* \frac{e^{-ikr_s}}{r_s} \frac{\sin(k|\mathbf{r} + \mathbf{r}_s|)}{k|\mathbf{r} + \mathbf{r}_s|} \tag{4.2}$$

and shows spherical illuminated spots with resolution $\sim k^{-1}$ centered at the atoms and their *twins*. The twins do not represent a problem in MEXH. In fact, as suggested by Barton[7], they can be mostly eliminated by integrating Eq. (4.1) over the energy as

$$U(\mathbf{r}) = \int U(\mathbf{r};\, k) e^{-ikr} \, k^2 dk$$

and we shall not discuss it. We shall concentrate on how to render f_s constant.

One way is to use the SWIFT method proposed by Saldin *et al.*[12]. In it, the Fourier transform Eq. (4.1) is done *not* on the *bare* hologram $\chi(\mathbf{k})$ as one gets from the data, but on the redefined quantity

$$\chi_{\rm SWIFT}(\mathbf{k};\,\mathbf{r}) = \frac{\chi(\mathbf{k})}{f_{\mathbf{r}}} \tag{4.3}$$

where

$$f_r = f_s(\hat{\mathbf{r}}_s \to \hat{\mathbf{r}})$$

and f_s is defined in Eq. (3.9). Using (3.8) one notes that as $\mathbf{r}$ in (4.1) approaches $\mathbf{r}_s$, $f_s/f_r \approx 1$, which guarantees that both shifts and distortions are eliminated in Eq. (4.1).

The method applies for any polarization, but problems may arise when the ratio $f_s/f_{\mathbf{r}}$ is $\sim 0/0$. In addition the dipole moments and the quadrupole term are assumed to be known.

Another way to render f_s constant, would be instead to use the bare experimental quantity $\chi(\mathbf{k})$, but to play with the polarization.

Neglect for the moment the corrections in (3.9) and concentrate on the first term only. To make the life easier, here and in the following we shall suppose that $\mathbf{p}$ is in the direction of the field. From this we define

$$f_s \sim |\boldsymbol{\epsilon}\times\hat{\mathbf{r}}_s|^2 = \sin^2\Psi, \tag{4.4}$$

and $f_s = 1$, if

$$\boldsymbol{\epsilon} \to \boldsymbol{\epsilon}_s = \frac{\hat{\mathbf{r}}_s\times\hat{\mathbf{k}}}{|\hat{\mathbf{r}}_s\times\hat{\mathbf{k}}|}. \tag{4.5}$$

The choice made in Eq. (4.5) implies the *a priori* knowledge of the position $\mathbf{r}_s$, but this can be roughly estimated through Eq. (4.1) and with an arbitrary polarization. The method we propose is the following.

Let $\boldsymbol{\epsilon}_1$, and $\boldsymbol{\epsilon}_2 = \hat{\mathbf{k}}\times\boldsymbol{\epsilon}_1$ be two polarizations where the second is obtained by a rotation of $\pi/2$ over the direction $\hat{\mathbf{k}}$ of the reference beam. Measure the yield for $\boldsymbol{\epsilon}_1$, $\boldsymbol{\epsilon}_2$ and for

$$\boldsymbol{\epsilon}_3 = \frac{1}{\sqrt{2}}\,(\boldsymbol{\epsilon}_1 + \boldsymbol{\epsilon}_2)$$

then call χ_1, χ_2 and χ_3 the respective holograms. The third measurement collects interference effects and constructs the hologram $\chi_{(\alpha,\beta)}$ for any polarization

$$\boldsymbol{\epsilon} = \alpha\boldsymbol{\epsilon}_1 + \beta\boldsymbol{\epsilon}_2 \quad ; \quad |\alpha|^2 + |\beta|^2 = 1 \tag{4.6a}$$

to be used in the experiment. For instance if both α and β are real one gets from (3.7a) the simple result

$$\chi_{(\alpha,\beta)} = (\alpha - \beta)(\alpha\chi_1 - \beta\chi_2) + 2\alpha\beta\chi_3. \tag{4.6b}$$

Taking for α and β the values

$$\alpha_s = \frac{\hat{\mathbf{r}}_s \cdot \boldsymbol{\epsilon}_2}{|\hat{\mathbf{r}}_s \times \hat{\mathbf{k}}|} \quad , \quad \beta_s = -\frac{\hat{\mathbf{r}}_s \cdot \boldsymbol{\epsilon}_1}{|\hat{\mathbf{r}}_s \times \hat{\mathbf{k}}|}, \tag{4.7}$$

$\boldsymbol{\epsilon} = \boldsymbol{\epsilon}_s$, thus $f_s = 1$ as wanted.

We show now with an example how, without corrections, distortion is effectively present. Suppose that $\mathbf{r}_s$ is along the z axis and take

$$\boldsymbol{\epsilon}_1 = \frac{\hat{\mathbf{z}} \times \hat{\mathbf{k}}}{|\hat{\mathbf{z}} \times \hat{\mathbf{k}}|}$$

in the (x, y) plane. Then $|\boldsymbol{\epsilon}_1 \times \mathbf{r}_s|^2 = 1$, but

$$|\boldsymbol{\epsilon}_2 \times \mathbf{r}_s|^2 = \cos^2\vartheta$$

where

$$\hat{\mathbf{k}} = (\sin\vartheta\cos\varphi,\, \sin\vartheta\sin\varphi,\, \cos\vartheta).$$

Spherical spots are insured for $\boldsymbol{\epsilon}_1$, but not for $\boldsymbol{\epsilon}_2$ as we now show.

Consider two paths: the first with $\mathbf{r}$ along z, and the second with $\mathbf{r} - \mathbf{r}_s$ in the (x, y) plane. For both paths the function U in Eq. (4.1) depends only on

$$\zeta = k|\mathbf{r} - \mathbf{r}_s|.$$

A simple calculation for the first path gives

$$U_{\parallel}(\zeta) = \frac{1}{\zeta}\left[\left(1 - \frac{2}{\zeta^2}\right)\sin\zeta + \frac{2}{\zeta}\cos\zeta\right]$$

with a maximum $U_{\parallel}(0) = 1/3$, and vanishing at

$$\zeta \approx \frac{\pi}{1.5}.$$

For the second path $U_\perp(0) = U_\parallel(0)$, but the shape is wider and vanishes at

$$\zeta \approx \frac{\pi}{.757}.$$

In this case then the illuminated spot is a highly anisotropic ellipse. The two axes of the ellipse are in the ratio $1.5/.757 \approx 2$.

V. NUMERICAL RESULTS AND CONCLUSIONS.

A numerical calculation has been carried out for a Fe bcc structure, to see how the method works. With the emitter at the origin, we limit our attention on the nearest neighbour spot $\mathbf{r}^* = (\frac{1}{2}\frac{1}{2}\frac{1}{2})a$, where $a = 2.87$ Åis the lattice spacing for iron. The plane is the $(1\bar{1}0)$ one and the directions [110] and [001] as indicated in the figures.

Fig. 2a is for polarization $\boldsymbol{\epsilon}_1$, here both orthogonal to $\hat{\mathbf{r}}^*$ and $\hat{\mathbf{k}}$ as in Eq. (4.5). A spherical spot is clearly shown, in spite of the possible disturbances induced by other scatterers, and neglected in the analysis of the previous section. Fig. 2b refers to $\boldsymbol{\epsilon}_2$ polarization, gotten by rotating $\boldsymbol{\epsilon}_1$ by $\pi/2$ around $\hat{\mathbf{k}}$ as indicated previously. Here the intensity is lowered and the anisotropy is present indeed. Both figures are for reference beam energy $E = 6.24$ KeV. The beam energy cannot be arbitrary, but must be chosen to avoid out of phase overlap between an atom and its twin, a well known problem in single-energy holography[8]. In fact the sum in Eq. (3.8) is invariant for $\mathbf{r}_s \to -\mathbf{r}_s$, thus one gets (apart from a $2k^2$ factor) the dimensionless quantity

$$\chi(\mathbf{k}) = \sum_s f_s \frac{\sin(kr_s)}{kr_s} \cos(\mathbf{k} \cdot \mathbf{r}_s), \tag{5.1}$$

with $f_s \leq 1$ for both polarizations given in Eq. (4.4). The prefactor $P = \sin(kr_s)/kr_s$ selects the possible energies for the image reconstruction as $\sin(kr^*) \approx +1$. Reversing the sign in defining the U function in Eq. (4.1), the values $\sin(kr^*) \approx -1$ are again possible, but we exclude them since are *minima* in the $|\mathbf{E}_{\rm Tot}|^2$ intensity in Eq. (3.7a). In the present case the

most suitable values for the image reconstruction for r^*-scatterer are $E_2 = 6.24$ KeV and $E_3 = 11.23$ KeV (the first value $E_1 = 1.25$ KeV being too small).

Figures 3a and 3b refer to this higher energy E_3. Again one notices that the r^*-atom is visualized only for $\boldsymbol{\epsilon}_1$ polarization (Fig. 3a), while this spot vanishes using the polarization $\boldsymbol{\epsilon}_2$ (Fig. 3b).

To get closer to the experimental conditions, the χ values in Eq. (5.1) have been calculated on a $5^\circ \times 5^\circ$-grid over the whole solid angle, then averaged over an experimental window. A *spline interpolation* on these grid–data creates the averaged hologram to be used under the integral in Eq. (4.1). In all cases we find that the angular averaging is irrelevant as far as $U(\mathbf{r})$ is concerned. The primary role is played by the integration over the modulus, i.e. over the energy. Here we use a 1–D gaussian convolution $g \sim \exp(-k^2/\Delta k^2)$ on the grid data. The effect of using the gaussian is twofold, and well discussed in Ref. [3]. On the one hand it is nothing but the energy spread of the primary beam. On the other, it acts as a low–pass filter to wash out all the distant scatterers, and at the same time avoids divergences in the reconstructed pattern. The first point is closely related to the dimension of the cluster, or *mutatis mutandis*, to the number of atoms of a *bulk* crystal we include under the sum in Eq. (3.8). We use a sphere of radius $R = a \times N$ and find that, for $\Delta k \approx \pi/(aM)$ and $N > M$, the result is independent of the sphere's radius.

There is however a divergence for large N, which has more to do with our definition of U than with the physics itself. It can be avoided when the integration is *not* performed overthe *whole* solid angle as in Eq. (4.1), but only on a part of it. This is what is usually done by the people working in atomic holography[13,14]. Nevertheless we shall continue to use Eq. (4.1), and show how to get rid of this problem.

Its origin can be figured out very simply by going to the scalar case, thus taking $f_s = 1$ constant. From Eq. (4.2) get the intensity at the origin

$$U(0) \to \sum_s \frac{\sin^2(kr_s)}{k^2 r_s^2} \sim R$$

which diverges for $R \to \infty$. The same trend is of course present for $|\mathbf{r}| \approx 0$, and this means

a very faint intensity in the whole pattern, except at the emitter. However, this divergence can be removed in the calculation by subtracting a C–constant, just as the *reference wave* is subtracted to get at the experimental χ. The C value we use is fixed by taking constant $U(0)$ as the sphere radius is increased from $R = a$ to $R = Na$. This is a very good way to check how the result stabilizes with increasing number of scatterers, even if other choices are possible[13].

We find much faster convergence at lower energy, as one would expect. The fourier transform (FT) $U(\mathbf{r})$ is smoother and the illuminated spots are larger.

Actually for $E = E_2$ we do *not* even need to perform a gaussian convolution, but only a *C–redefinition* of the type discussed is required. Nevertheless an energy spread is used in all the figures we present. We fix $\sigma = \Delta k/k = 6.411 \times 10^{-2}$, close to the Tegze and Feigel[3] value, this being the *default* value for $R \gtrsim 3a$, and energy E_3. We have checked, as just noted, that Figs. 2a and 2b remain in practice the same using a larger σ or setting $\Delta k = 0$ (monocromatic beam). On the contrary, in Fig. 3a and Fig. 3b a gaussian convolution is essential.

The numerical calculation is performed with a *Fortran* program. Once the averaged holograms χ_1, χ_2 and χ_3 are calculated on the $5^\circ \times 5^\circ$ grid, the FT requires 2' and 30" of computer time for each reconstruction at $E = 11.23$ KeV. For Figs. 2a, 2b the requirement reduces to $\sim 1'$. For the graphical part we use *Mathematica*. To get better contrast in the figures, we follow the standard procedure used in atomic holography[14], namely plotting $|U|^2$ rather then $|U|$. Before doing this U has been redefined such that $0 \leq U \leq 1$ in the whole $0 \leq x \leq \sqrt{2}a$, $0 \leq y \leq a$ $(1\bar{1}, 0)$ plane, or in the relevant part of it.

In conclusion, we can assert that the reconstruction of the image can be gotten with a reasonable effort from the experimental hologram. The energy spread of the nearly monochromatic reference beam, prevents to see distant scatterers, but justifies to neglect the *self-hologram* contribution. An additional convolution of the data with a gaussian lowers the definition of the image, but makes the *self-hologram* even smaller. The polarization, together with the energy, plays an essential role for the observability of the atom. The polarization

‘ *constraint* ’ remains effective even if, as in MEXH, the integration over energy is performed.

ACKNOWLEDGMENTS

One of us (A. M. M.) would like to thank L. Fonda for stimulating discussions on this subject. We thank J.S. Frasier for a critical reading of the manuscript and help with editing it.

REFERENCES

[1] D. Gabor, Nature (London) **161**, 177 (1948); Proc. R. Soc. London, Ser. A **197**, 454 (1949); Proc. Phys. Soc., London, Sect. B **64**, 449 (1951).

[2] A. Szöke, Short Wavelength Coherent Radiation, in Am. Inst. of Phys. Conf. Proc. **147**, 361 (1986).

[3] M. Tegze and G. Faigel, Europhys. Lett. **16**, 41 (1991); Nature (London) **380**, 49 (1996).

[4] P. M. Len *et al.*, Phys. Rev. B **50**, 17 463 (1994).

[5] J. J. Barton, Phys,. Rev. Lett. **61**, 1356 (1988).

[6] T. Gog, P. M. Len, G. Materlik, D. Bahr, C. S. Fadley, and C. Sanchez-Hanke, Phys. Rev. Lett. **76**, 3132 (1996).

[7] J. J. Barton, Phys. Rev. Lett. **67**, 3106 (1991).

[8] P. M. Len, T. Gog, C. S. Fadley, and G. Materlik, Phys. Rev. B **55**, R3323 (1997).

[9] L. D. Landau and E. M. Lifshitz, Quantum Mechanics, Ch. 6, § 40.

[10] L. Fonda, Phys. Status Solidi B **201**, 329 (1997).

[11] J. J. Jackson, *Classical Electrodynamics* 2nd Ed. (J. Wiley & Sons, New York, 1975), Sect. 9.2, p. 394.

[12] D. K. Saldin, G. R. Harp, and B. P. Tonner, Phys. Rev. **B 45**, 9629 (1992).

[13] P. M. Len, Ph.D. Thesis (1997), *unpub.*

[14] P. M. Len, *private comm.*

FIGURES

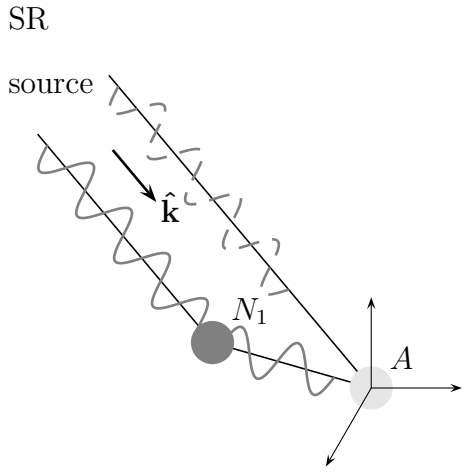

FIG. 1. The picture of MEXH process. The interference pattern is due to the different optical paths of the direct beam (dashed) and the one scattered by the neighbouring atom N_1 (solid line).

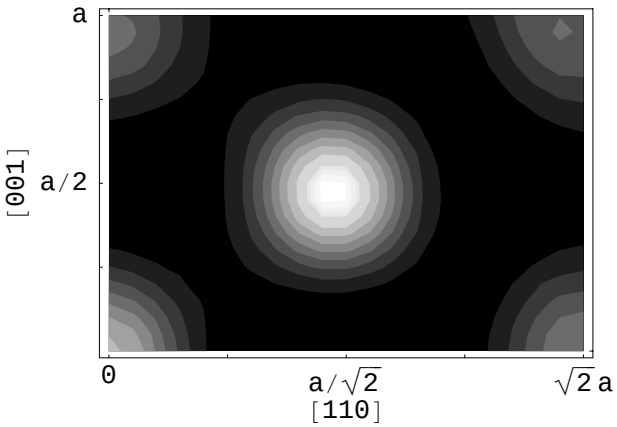

FIG. 2a. Theoretically generated atomic images for a Fe bcc crystal on the $(1\bar{1}0)$ plane. The X-ray energy is $E = 6.24$ KeV and the polarization $\boldsymbol{\epsilon}_1$ is defined in the text. Other parameters are $R = 3a$ (258 scatterers), $C = .273$, and $\Delta k/k = .064$ for the gaussian convolution.

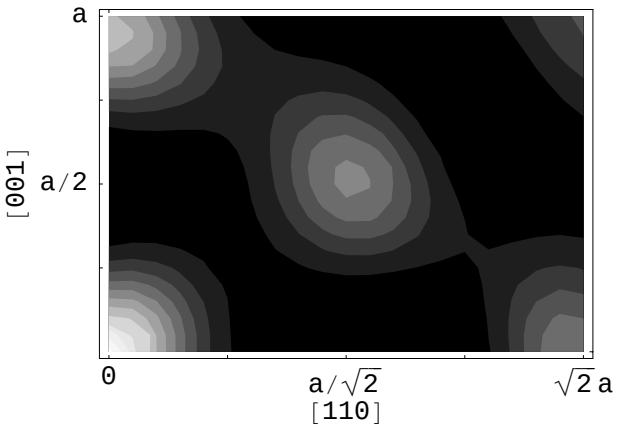

FIG. 2b. As in Fig. 2a, but for the $\boldsymbol{\epsilon}_2$ polarization.

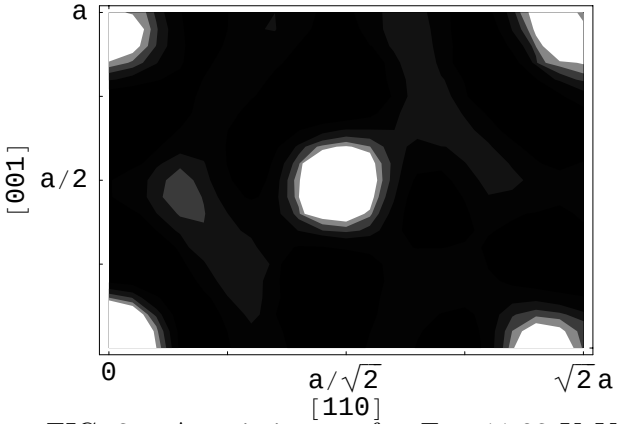

FIG. 3a. Atomic images for $E = 11.23$ KeV and polarization $\boldsymbol{\epsilon}_1$. Here we have used $R = 4a$ (536 scatterers), $C = .132$, and the same $\Delta k/k$.

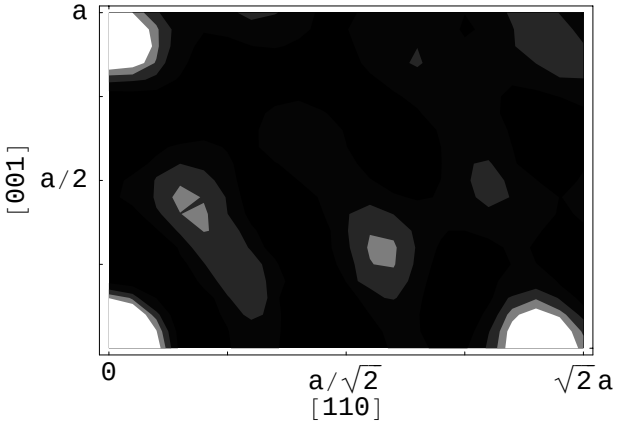

FIG. 3b. As in Fig. 3a, but for $\boldsymbol{\epsilon}_2$ polarization.